Published June 27, 2017

RESEARCH

Application of Geographically Weighted Regression to Improve Grain Yield Prediction from Unmanned Aerial System Imagery

Atena Haghighattalab, Jared Crain, Suchismita Mondal, Jessica Rutkoski, Ravi Prakash Singh, and Jesse Poland*

ABSTRACT

Phenological data are important ratings of the in-season growth of crops, though this assessment is generally limited at both spatial and temporal levels during the crop cycle for large breeding nurseries. Unmanned aerial systems (UAS) have the potential to provide high spatial and temporal resolution for phenotyping tens of thousands of small field plots without requiring substantial investments in time, cost, and labor. The objective of this research was to determine whether an accurate remote sensing-based method could be developed to estimate grain yield using aerial imagery in small-plot wheat (*Triticum aestivum* L.) yield evaluation trials. The UAS consisted of a modified consumer-grade camera mounted on a low-cost unmanned aerial vehicle and was deployed multiple times throughout the growing season in yield trials of advanced breeding lines with irrigated and drought-stressed environments at the International Maize and Wheat Improvement Center in Ciudad Obregon, Sonora, Mexico. We assessed data quality and evaluated the potential to predict grain yield on a plot level by examining the relationships between information derived from UAS imagery and the grain yield. Using geographically weighted (GW) models, we predicted grain yield for both environments. The relationship between measured phenotypic traits derived from imagery and grain yield was highly correlated (r = 0.74 and r = 0.46 [$p < 0.001$] for drought and irrigated environments, respectively). Residuals from GW models were lower and less spatially dependent than methods using principal component regression, suggesting the superiority of spatially corrected models. These results show that vegetation indices collected from high-throughput UAS imagery can be used to predict grain and for selection decisions, as well as to enhance genomic selection models.

A. Haghiaghattalab, J. Crain, and J. Poland, Dep. of Plant Pathology, Kansas State Univ., Manhattan, KS 66506; S. Mondal and R.P. Singh, International Maize and Wheat Improvement Center (CIMMYT), Int. Apdo. Postal 6-641, 06600, Mexico D.F.; J. Rutkoski, International Rice Research Institute, DAPO Box 7777, Metro Manila, 1301, Philippines; J. Poland, Wheat Genetics Resource Center, Dep. of Plant Pathology and Dep. of Agronomy, Kansas State Univ., Manhattan, KS 66506. Received 22 Dec. 2016. Accepted 23 Apr. 2017. *Corresponding author (jpoland@ksu.edu). Assigned to Associate Editor Carlos Messina.

Abbreviations: AIC, Akaike's information criterion; BNDVI, blue normalized difference vegetation index; DEM, digital elevation model; DSM, digital surface model; DTM, digital terrain model; ENDVI, enhanced normalized difference vegetation index; GCP, ground control point; GIPVI, green infrared percentage vegetation index; GNDVI, green normalized difference vegetation index; GW, geographically weighted; GWR, geographically weighted regression; HTP, high-throughput phenotyping; NDVI, normalized difference vegetation index; PCR, principal component regression; UAV, unmanned aerial vehicle; UAS, unmanned aerial system; VI, vegetation index.

Wheat (*Triticum aestivum* L.) is a primary staple crop throughout the world, with a total projected production of 727 million metric tons in 2016 (USDA, 2016). Due to the emergence of more aggressive pests and diseases, shortage of available water resources, lack of fertile soil, and climate change, wheat production is projected to fall behind the increasing demand (Ray et al., 2013). With limited options to increase the amount of land under production, it is generally agreed that increasing crop yield per unit area, rather than expanding cultivated land area, is needed to meet the world demand for wheat by 2050 (Muir et al., 2010; Foley et al., 2011). A rate of gain per year of 2% or more is needed to meet the projected targets (Ray et al., 2013), whereas most studies estimate the current rate of genetic increase at 1% or less (Reynolds et al., 2012). Thus,

Published in Crop Sci. 57:2478–2489 (2017).
doi: 10.2135/cropsci2016.12.1016

substantial investments and deployment of new tools in plant breeding programs are needed.

Several studies have indicated that breeding programs must substantially increase or even double the rate of variety development and improvement to increase crop yield at a sufficient pace to meet growing demands (Reynolds et al., 2009; Tester and Langridge, 2010). Theoretically, any gains in plant breeding can be summarized from the breeders equation, which is a function of the additive genetic variance, trait heritability, selection intensity, and breeding cycle time (Falconer and Mackay, 1996; De La Fuente et al., 2013). A critical part of traditional phenotypic selection involves the use of manual data collection that is time consuming, labor intensive, expensive, and often burdensome or limited when making selections in large populations. The precision of the data collected directly relates to the accuracy of selection by correctly partitioning environmental and genetic variance. Although there have been few changes in phenotypic tools and evaluation methods (White et al., 2012), astonishing advances over the last 5 to 10 yr have occurred in sequencing technology, resulting in many advanced tools and methods to assess genotypes and improve plant breeding techniques through genomics and reducing the time of the breeding cycle (Elshire et al., 2011; White et al., 2012; Cobb et al., 2013). The grand challenge remains in measuring plant phenotypes with the same speed and precision as is possible for observing the genome. This has led to active innovation in field-based high-throughput phenotyping (HTP) platforms.

High-throughput phenotyping platforms could provide the keys to connecting genotype to phenotype by increasing the capacity, efficiency, and precision of evaluating large plant populations. Due to potentially rapid measurements, HTP can increase the population sizes screened for desirable traits in breeding nurseries. An increase in population size enabled by HTP increases the probability of identifying valuable traits and the genetic bases of those traits. Related to the breeders equation, a breeding program can achieve a higher capacity through genetic gain by increasing the intensity and accuracy of selection (Goggin et al., 2015; Poland, 2015; Reynolds and Langridge, 2016).

The precision and accuracy with which these traits can be measured is also expected to increase using HTP compared with manual measurements (White et al., 2012; Goggin et al., 2015). The emphasis on high dimensionality and the need for automation and more nondestructive sampling techniques in general necessitate that HTP platforms often rely on imaging to measure plant phenotypes (Goggin et al., 2015). One emerging technology allowing plant breeders to screen large numbers of genotypes rapidly is unmanned aerial systems (UAS). The main advantage of UAS over traditional manual approaches is the ability to cover an entire experiment area in a very short time, enabling researchers to monitor larger fields with higher temporal resolution and higher spatial resolution during the growing season.

Different imaging systems are being used on unmanned aerial vehicle (UAV) phenotyping platforms, making them capable of generating various measurements useful for plant breeding programs (White et al., 2012; Deery et al., 2014; Liebisch et al., 2015). High-resolution multispectral cameras can be used to produce three-dimensional models of the experiment area, resulting in the extraction of plant height using a digital elevation model (DEM) that determines height as the difference between the digital surface model (DSM) and the digital terrain model (DTM) (Rosnell and Honkavaara, 2012; Feng et al., 2015). Other sensors include hyperspectral and thermal cameras that can be used to investigate different vegetation indices (VIs) or canopy temperatures and their relation to crop biomass and yield (Hruska et al., 2012).

Several spectral reflectance measurements and VIs have shown a strong relationship to plant health and crop growth. From this, remote sensing has proven to be a valuable tool for estimating crop yield in advance of harvest. One of the most common VIs, the normalized difference VI (NDVI), has been used by researchers for crop yield predictions since the 1980s (Singh et al., 2001; Teal et al., 2006; Sultana et al., 2014; Wang et al., 2014). In a study conducted by Salazar et al. (2007), a strong correlation was found between winter wheat yield and NDVI extracted from satellite imagery during the critical period of development and productivity occurring during April to May in Kansas. Grain yield prediction using remote sensing has been extensively studied in cereal crops such as wheat using satellite and aerial imagery (Manjunath et al., 2002; Prasad et al., 2006; Salazar et al., 2007; Mkhabela et al., 2011; Rutkoski et al., 2016a) or ground-based platforms (Raun et al., 2001; Rischbeck et al., 2016). However, little work has been conducted using UAV platforms.

The use of physiological measurements to predict grain yield is an indirect selection approach proposed and implemented in wheat breeding (Babar et al., 2006b; Crain et al., 2016; Rutkoski et al., 2016b). Vegetation indices have been widely studied as the potential tool to differentiate genotypes for yield under different environmental growing conditions, such as irrigated and nonirrigated (Arnold et al., 1995; Babar et al., 2006a; Araya et al., 2013; You et al., 2013). Additionally, several studies have examined how yield-enhancing traits, such as stay-green, can be used as a predictor of grain yield using spectral responses. Lopes and Reynolds (2012) studied temporal NDVI data from grain fill to maturity to improve understanding of genotypic stay-green variation. In this study, they found that stay-green variables explained 30% of yield variability in multiple regression analysis, although the cumulative effect that stay-green variables provide, together with

other traits, may allow for additional insights to be gained about plant health and final grain yield.

Data derived from HTP can provide deeper and broader insight into the crop growth, development, and performance than what is currently available to breeders. With the addition of georeferenced and spatial data inherent in HTP and imagery, researchers can utilize tools not traditionally used in the area of plant breeding, including spatial modeling commonly applied in geospatial sciences. The purpose of this research was to evaluate the performance of geographically weighted (GW) models in predicting grain yields at the plot level in breeding nurseries. The foundation of geostatistical rationale is the understanding that spatial data, information about the locations and shapes of geographic features (wheat plots), and the relationships between them, stored as coordinates and topology, will vary across a field (Mitchell, 2005). Regression-based models mostly ignore this assumption, which could potentially affect the accuracy of prediction models.

In this scope, a typical multiple linear regression model follows:

$$\gamma_i = \beta_0 + \sum_{j=1,m} \beta_j x_{ij} + \varepsilon_i \qquad [1]$$

where γ_i is the ith observation of the dependent variable, x_{ij} the ith observation of the jth independent variables, and ε_i the residual that is identically and independently distributed. When applied to spatial data, this model assumes a stationary spatial process (spatially consistent relationships between the dependent variable and each explanatory variable across the field) and produces one single model for all parts of the study area. Field trials, however, are inherently spatial, typically having spatial trends across the field that will affect the accuracy of these models.

Along with typical linear regression, other statistical measures have been proposed to alleviate the challenges of spatial data. The application of mixed models to spatial data has generally resulted in improved accuracy and efficiency (Gilmour et al., 1997). Even with these improvements, geostatistical mixed model analysis like kriging still assumes that spatial variation in the phenomenon is statistically homogeneous and the same pattern of variation can be observed at all locations (Oliver and Webster, 2015).

Geographically weighted regression (GWR) is a local statistical approach to model spatially heterogeneous processes, which could be applicable to field trials. This regression model is used to analyze spatial nonstationarity—when the extent of relationships among variables differs from location to location (Brunsdon et al., 1996; Fotheringham et al., 2002; Lu et al., 2014a). For example, in field trials, the location refers to the distance between plots within one experiment rather than to multisite or multienvironment trials. In this approach, unlike other regression models, the spatial nonstationary relationship is assumed and is tested, according to Tobler's first law of geography: everything is related to everything else, but near things are more related than distant things (Tobler, 1970). Continuing the above example, plots located on the far north end of the experiment would be assumed to be more like plots located (closer distance) in the northern area of the experiment than plots at the southern end. Geographically weighted regression allows the relationships to vary over space and extends the traditional regression framework of Eq. [1] by allowing local variations in rates of change so the coefficients in the model are no longer global estimates but are specific to a location i. This is the core of GWR, in the linear form:

$$\gamma_i = \beta_{i0} + \sum_{j=1,m} \beta_{ij} x_{ij} + \varepsilon_i \qquad [2]$$

where β_{ij} is the value of the jth parameter at location i. Instead of remaining the same everywhere, β_{ij} now varies in terms of the location (i) (Brunsdon et al., 1996; Fotheringham et al., 2002; Mennis, 2006; Lu et al., 2014a). Although GWR should allow more flexibility of modeling, there has been limited application of the technique in agriculture and plant breeding. One agricultural example of GWR, in comparison with spatial analysis of regression kriging, showed that GWR resulted in lower root mean squared error and higher accuracies than regression kriging (Wang et al., 2012)

In the context of growing interest in UAS applied to precision agriculture studies, we evaluated the relationship between grain yield and the data extracted from UAS imagery, including green NDVI (GNDVI), blue NDVI (BNDVI), enhanced NDVI (ENDVI), green infrared percentage VI (GIPVI), and plant height during the growing season. Using the extracted data, we evaluated the application of spatiotemporal UAS imagery to predict within-season grain yield in a large international wheat breeding program using GWR and compared those results with principal component regression (PCR) of the same data. Principal component regression is a popular technique that can adequately account for multiple variables that may have varying levels of correlation between variables (Mevik and Wehrens, 2007).

MATERIALS AND METHODS

Study Area

The study was conducted at Norman E. Borlaug Experiment Station at Ciudad Obregon, Sonora, Mexico, in two different growing environments, drought and irrigated. The genetic materials were advanced breeding lines in the advanced yield trials of the CIMMYT bread wheat breeding program. The experiment consisted of 280 advanced wheat lines distributed in 10 trials, with each trial consisting of 28 entries and two

checks. Each trial was arranged as an α lattice design with three replications and six blocks per replication. The different environments were based on megaenvironments, which are major wheat-growing regions that experience similar growing environments, with the tested environments of drought and irrigated representing ~10 and 32 million ha worldwide, respectively (Braun et al., 1996). The plot size for each experimental unit in irrigated trials was 2.8 m long and 1.6 m wide (plot area = 4.48 m^2) sown on two 0.8-m-wide raised beds with two rows per bed, whereas plots in drought trials were 4 m long and 1.3 m wide (plot area = 5.2 m^2) sown on flat land as six rows 18 cm apart with 40-cm interplot spacing. The drought trial was sown at the optimum planting date with minimal irrigation throughout the season using drip tape. The irrigated environment represents an optimal planting date (mid-November) with optimal flood irrigation throughout the growing season. During the crop season, the drought environment received 180 mm of irrigation, and the irrigated environment received 500 mm of water. Fertilizer and pesticide control were similar in both environments.

Platforms and Cameras

High-throughput phenotypic data from a UAS were collected as previously described by Haghighattalab et al. (2016). Briefly, we used a consumer-grade Canon S100 camera modified by MaxMax (LDP) to collect blue, green, and near-infrared light. The camera was mounted on a low-cost UAV, (IRIS+, 3D Robotics) with a custom-designed gimbal to allow for nadir image collection. Supplemental Table 1 contains detailed specifications for instruments used to collect data.

Ground Control Points and Reflectance Calibration Panel

To georeference the aerial images, 13 ground control points (GCPs) were distributed across each field at the beginning of the season. The GCPs coordinates were measured with a Trimble R4 RTK GPS that has a horizontal accuracy of 2.5 cm and a vertical accuracy of 3.5 cm. These targets were maintained throughout the crop season to enable the overlay of measurements from multiple dates. The GCPs were designed as coded targets (printed as circles with black and white segments) on 25-cm × 25-cm square white metal sheets and mounted on a 50-cm post to provide easy identification of GCPs in the image processing software. Six white 30-cm × 30-cm square ceramic tiles mounted on 10-cm blocks were also used to have a variety of heights in GCPs to increase the accuracy of height extraction analysis.

To enable consistent analysis of extracted data from aerial imagery across multiple days, we placed a calibration panel in the field before each flight. This foldable panel consisted of six individual 7-mm-thick lightweight plywood panels with levels of gray, from 0 (white) to 100% (black), and were attached using metal hinges. Using a handheld spectroradiometer (ASD) on a sunny day, the spectral reflectance of these panels were measured at a fixed height of 50 cm from five different angles. We also used this panel for white balance adjustment of the raw imagery captured by our consumer-grade camera.

Field Data Collection

At maturity, the whole plot was harvested to estimate grain yield in tons per hectare. For the irrigated environment, manual measurements for plant height were recorded for the first replicate in each trial (n = 300) and for all plots in the drought environment (n = 900). These measurements were taken as the distance from the ground to the average top of the terminal spikelet for a representative plant, usually from the middle of the plots. Before measurement, culms were manually pulled up to the vertical position if they were lodged (Bell et al., 1994).

For each environment, aerial imagery was taken at multiple time points using the UAV phenotyping platform (IRIS+ and a modified Canon S100 camera) during the growing season, with observation days spaced at ~7-d intervals, depending on the weather condition. All images were taken in RAW format (.CR2) to avoid loss of image information. An overview of each day of UAS observation is summarized in Table 1.

HTP Image Processing

For each experiment, we collected three sets of observations from heading through senescence (Zadoks et al., 1974). The semiautomated data analysis pipeline presented in Haghighattalab et al. (2016) was used to analyze each dataset and extract plot-level phenomics values. Image processing was primarily conducted using Python scripts described and available from Haghighattalab (2014, 2015), open-source software QGIS (QGIS Development Team, 2015), and Agisoft PhotoScan package (Agisoft, 2016).

To generate plot-level values for VIs and plant height, the image processing developed by Haghighattalab et al. (2016) was used. In summary, HTP data processing for each time point of data collection included the following steps:

1. Preprocess raw images.
2. Perform camera alignment.
3. Import and reference GCPs.
4. Optimize GCP alignment.
5. Construct a dense point cloud.
6. Classify the data within the dense point cloud as plant or soil.
7. Build a DEM using the classified point cloud.
8. Form an orthomosaic image using two different blending methods.
9. Generate an orthomosaic and DEM.
10. Calculate the various VIs and plant height.
11. Extract the plot-level data.

Due to the available bandwidths using the modified Canon S100, the calculated VIs were limited to GNDVI, BNDVI, ENDVI, and GIPVI. The following formulas were used to calculate each index: BNDVI = (NIR − Blue)/(NIR + Blue); GNDVI = (NIR − Green)/(NIR + Green); ENDVI = [NIR + Green − (2 × Blue)]/[NIR + Green + (2 × Blue)]; GIPVI = NIR/(NIR + Green).

Plant Height Extraction

PhotoScan generates a dense point cloud using the estimated camera positions. The program also calculates depth

Table 1. Flight information using unmanned aerial system high-throughput phenotyping platform (IRIS+ and modified Canon S100) at CIMMYT, Ciudad Obregon, Mexico, in 2016.

Environment	No. of flights	Flight speed	Altitude	Overlap of each photo		No. of images	Spatial resolution
				Side	Forward		
		m s^{-1}	m	%			cm
Drought	3	2	30	70	80	100	~0.9
Irrigated	3	2	25	70	80	93	~0.9

information for each photo to be combined into a single dense point cloud (Agisoft, 2016). Dense point clouds with high accuracy were generated where the user has the option to specify the level of detail. Using high-level accuracy resulted in DEM with accuracy of 1.83 and 1.79 cm pixel^{-1} for the drought and irrigated trials, respectively.

To extract plant height, both the DTM and the DSM were produced, with plant height being calculated as the difference between these two models:

$$\text{Plant height} = \text{DSM} - \text{DTM} \quad [3]$$

The generated dense point cloud includes everything that can be seen in the images, pixels from the ground, vegetation, and any other artifacts or noise. PhotoScan offers two options of dense point cloud classification: (i) automatic classification of the points into two categories, ground points and other; and (ii) manual selection of a group of points to be placed in a particular class from the standard list known for light detection and ranging (LIDAR) data, such as vegetation, water, or road surface. Three parameters control automatic ground point classification: maximum angle, maximum distance, and maximum cell size (Agisoft, 2016). Point cloud classification provides ways to customize the DEM generation step, as the software allows users to choose types of objects within the scene to be reconstructed and to indicate the corresponding point class as a source data for DEM generation. For example, DEM reconstruction based on ground points only allows users to export DTM (as opposed to DSM based on the complete dense point cloud, excluding the artifacts and noises) (Agisoft, 2016).

In the plot imagery, the default values for maximum angle and maximum distance parameter values were reduced, since the heights of crops are considerably lower than heights of other objects like buildings. To estimate plant height, automatic classification of ground points was performed, followed by manual classification of vegetation points, generating DTM and DSM for each dataset. Training sets for classes of "ground," "low vegetation," and "high vegetation" were defined by sampling the points. Using the classified point cloud, the DTM was extracted using only ground points, and the DSM using data assigned to the vegetation points. For a small field, the generated classified point cloud can be used to calculate plant height directly. However, the point cloud exported from PhotoScan contains very large files, and for large wheat breeding nurseries, as used in our study, the generated DEM was used.

Using our custom field map-based method, two plot boundaries for each field were extracted. One plot boundary was buffered to avoid pixels outside the plot and was used for the DSM extraction, as we are only interested in values reflected from wheat plants. The second plot boundary was extended to have the DTM values of the ground surrounding the wheat plots. Mean, SD for DSM, and lower quantile (25%) for DTM were calculated. Height was calculated for each plot as the difference between the mean values of DSM and lower quantile values of DTM, as these values best represent the ground elevation point in the DTM.

Using the classified DEM, orthomosaics using both blending methods (average and mosaic) were generated. In the average mode, the brightness values of the final orthomosaic is the average of all the overlapping images, whereas mosaic mode only uses the pixel value from the image taken from the most nadir view of that given point (Agisoft, 2016; Haghighattalab et al., 2016).

As described in our developed pipeline, after calibrating each orthomosaic dataset for each environment using the empirical line method, VI maps using open-source software QGIS were generated (Smith and Milton, 1999; Haghighattalab et al., 2016). Statistical values for each plot for each day of data were calculated that included the minimum, mean, maximum, and SD for both blending methods.

HTP Data Analysis

Broad-Sense Heritability

Within environment and trial, broad-sense heritability was calculated on a line-mean basis within environment, commonly known as repeatability (Piepho and Möhring, 2007), for extracted VIs measured on individual dates and grain yield. To estimate heritability, a two-step process was performed where we first calculated the plot-level value for HTP measurements and then fit a mixed model for replicate, block nested within replicate, and genotype as random effects. Broad-sense heritability for each trait within trial within environment was calculated from Eq. [4] (Holland et al., 2003):

$$H^2 = \frac{\sigma^2_{\text{genotypic}}}{\sigma^2_{\text{genotypic}} + \frac{\sigma^2_{\text{error}}}{\text{nrep}}} \quad [4]$$

where $\sigma^2_{\text{genotypic}}$ is genotypic variance, σ^2_{error} is error variance, and nrep is the number of replicates in the trial (nrep = 3). The *lme4* R package was used for all mixed model analysis (Bates et al., 2014).

Parameter Estimation

Because the phenotypic VIs were highly correlated, PCR was used to evaluate the relationship between phenotypic values and grain yield (Supplemental Tables 2 and 3). Principal component analysis allowed all measured variables to contribute to the model, in comparison with multiple linear regression techniques that would succumb to collinearity (between VIs and dates) or only use a few variables through stepwise regression. Within each environment, a PCR model was fit using the plot level multi-temporal and multi-VI (ENDVI, BNDVI,

GIPVI, GNDVI) to observed grain yield. The *pls* R package (Mevik et al., 2013) was used for all principal component model development, and the first six principal components from each environment were used, as they represented >90% of the variation within each dataset. The height measurements were assessed by calculating the correlation between manual height measurements and extracted UAS imagery measurements.

Geographically Weighted Modeling

By mapping yield and VIs from both growing conditions, the presence of spatial patterns were observed (Fig. 1). This led us to develop a GW model to explore changing spatial relationships between grain yield and measured phenotypic traits. An important extension of GWR is its semiparametric construction by combining globally fixed and geographically varying coefficients (Lu et al., 2014b):

$$y_i = \sum_k \beta_k(u_i, v_i) x_{k,i} + \sum_l \gamma_l + z_{l,i} + \varepsilon_i \quad [5]$$

where y_i, $x_{k,i}$, and ε_i are grain yield, kth phenotypic trait (phenotypic traits include VIs and plant height), and the Gaussian error at location i, respectively; (u_i, v_i) is the x-y coordinate of the ith location; and coefficients $\beta_k(u_i, v_i)$ are varying conditionals on the location. The global term $z_{l,i}$ is the lth phenotypic trait with a fixed coefficient γ_l (Nakaya, 2016).

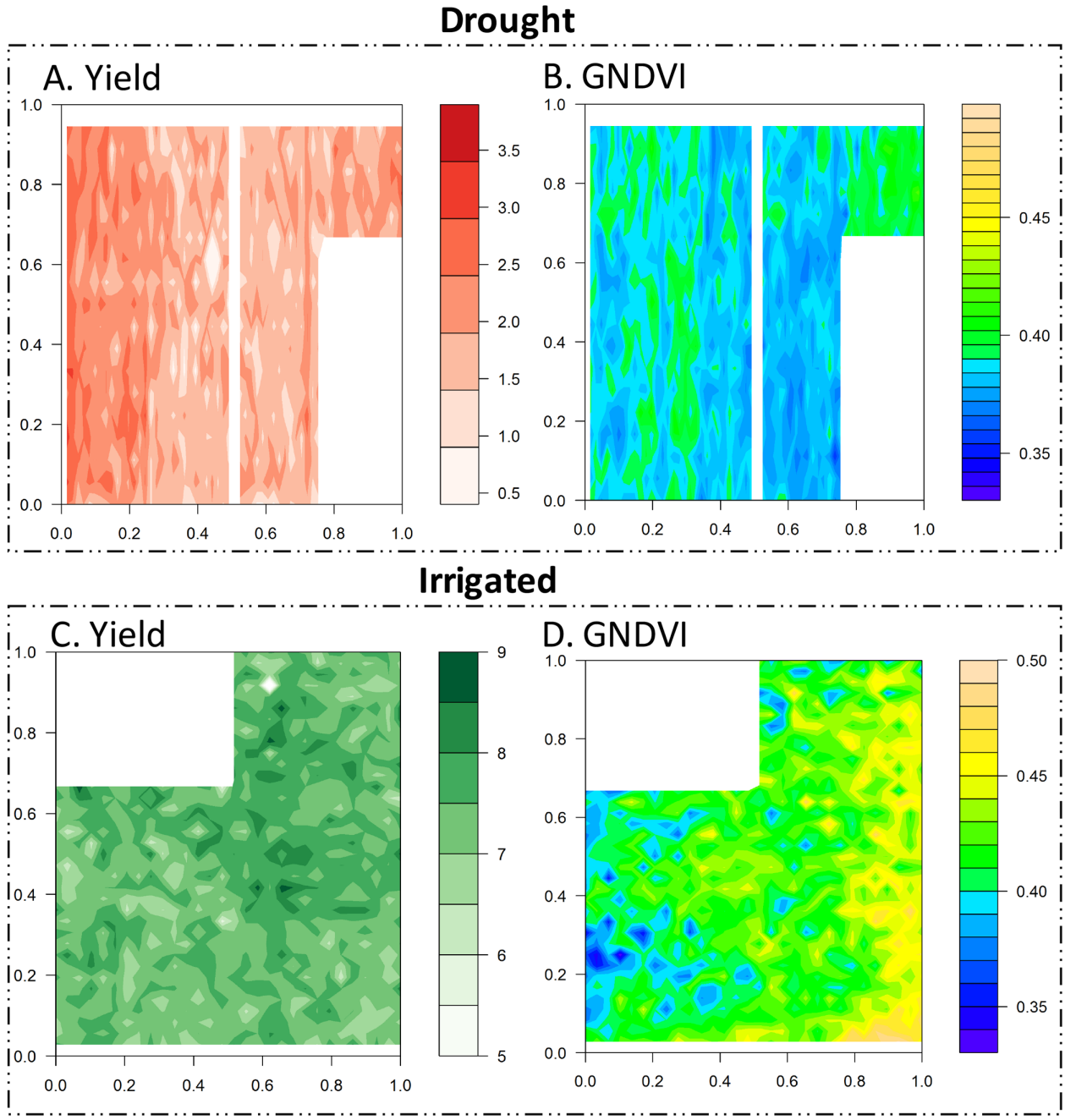

Fig. 1. (A) Mapping yield values in the drought environment shows the spatial variation across the field from left to right. Yield is reported in tons per hectare. (B) The heatmap of green normalized difference vegetation index (GNDVI) values for drought in 10 Mar. 2016. (C) The yield values in irrigated environment show patches of spatial variation across the field, although less variation than the yield in drought, with yield reported in tons per hectare. (D) Map of GNDVI values for the irrigated environment, 10 Mar. 2016.

In this approach, a moving window weighting technique is used where local models at both sampled and unsampled locations are calibrated. All neighboring observations for an individual sample point are weighted based on a distance decay kernel function, and the model is fit to this weighted data. The key to GW modeling is the weighting matrix, which sets the spatial dependency in the data (Lu et al., 2014b). There are three elements in defining this matrix: the distance metric, the type of kernel weighting function, and the kernel weighting function's bandwidth, which controls the size of the moving window (Mennis, 2006). The scope of these parameters and details on GW modeling are outlined in Fotheringham et al. (2002).

For the distance metric in this study, the distance between polygon centroids of the spatially defined field plots was used. An adaptive kernel function was used, and an optimal bandwidth was selected by minimizing Akaike's information criterion (AIC) (Kupfer and Farris, 2007). The adaptive bandwidth approach was chosen to account for the varying distance among wheat plot centroids due to (i) longer veritical than horizontal distance between plots (e.g., rectangle shapped plots), and (ii) larger gaps between section and trials boarders (Mennis, 2006).

For GW modeling, the GWmodel package in R was used to investigate spatial relationships among the numerous phenotypic observations and grain yield (Lu et al., 2014b).

Model Assessment

The prediction models for PCR and GWR were validated using a 10-fold cross validation with the accuracy of prediction reported as the correlation of the predicted values compared with the observed values. We used individual trials as folds, with nine trials choosen and placed in a training set, and the final fold or trial was predicted using the model developed from the training set. This was repeated 10 times across all trials to predict every plot. This particular cross validation takes advantage of the fact that genotypes were assigned to trials with closer related lines evaluated in the same trial. Using folds that correspond to trials reduced bias from closely related genotypes in both the training and validation sets, as full-sib lines are planted together in the same trial for these nurseries.

RESULTS AND DISCUSSION

Image Processing for HTP Data

To evaluate the potential of UAS for within-season grain yield prediction in wheat breeding programs, a low-cost, consumer-grade UAV phenotyping platform was deployed at multiple times throughout the growing season in two different growing environments (Table 1). The imagery taken at various dates was processed using a semi-automated pipeline (Haghighattalab et al., 2016). Image processing included converting raw imagery to TIFF format, georeferencing, point cloud generation, DEM and orthomosaic generation, and plot-level data extraction. We examined how the choice of mosaic or average orthomosaics generation affected the results. Additionally, our pipeline calculated the standard summaries for each plot of minimum, maximum, mean, range, and SD of each VI. The pipeline made efficient use of the data that were generated. For a regular flight, 100 photos were taken, resulting in 1.35 GB of raw data, and processing time averaged 3 h flight^{-1} on a 16-GB RAM single-core processor. While efficient, this highlights one of the needed areas of research—to reduce processing time to allow users to collect data and rapidly analyze or even process data in real time on larger and larger datasets.

Plant Height Measurements

To evaluate the suitability of using the UAS phenotyping platform to monitor plant height, the pairwise correlation was calculated between manual measurements and the height extracted from UAS for the drought and irrigated environments (n = 900 for drought, and n = 300 for irrigated). Using the initial data, it was apparent that there were outliers in both the drought and irrigated environment due to lodging. Using the SD of the height values calculated from the DEM for both environments, a minimum height threshold was set to identify and remove lodged plots. After removal of plots with height <60 cm for drought environment and 80 cm for irrigated environment, there was a significant correlation between height extracted from the DEM and manual measurements of height with correlations of r = 0.56 ($p < 0.001$, n = 870) and r = 0.70 ($p < 0.001$, n = 288) for drought and irrigated, respectively (Fig. 2).

While we found a significant association between manual measurements and UAS height measurement, we believe the results for height could be improved with an elevation map taken before vegetation begins growing. This would be a more accurate DEM map of the area and allow for more precise height extractions from the DTM. Additionally, we found that relying on the minimum values or the lower quantile values of DTM extracted from each plot of wheat was more challenging for the irrigated environment, since irrigated trials were planted in beds.

The lower correlation with manual measurements for the drought environment versus the irrigated environment is likely due to the narrow range of only 16 cm (SD of manual measurements: 4.7 cm) in plant height in drought environments (68–84 cm for 900 observed plots), compared with a range of 31 cm (SD = 3.0 cm) for irrigated environments (91–122 cm for 300 plots). Additionally, the manual measurements may also contain human error and bias from choosing representative plants and rounding results to a full centimeter, further diluting the precision of evaluation between manual and UAS height measurements.

Grain Yield Prediction Using Principal Component Regression

To evaluate the potential of UAS phenotyping platforms to quantify grain yield, PCR was used to develop models for each environment. This technique provides a method to adequately address the correlation between variables,

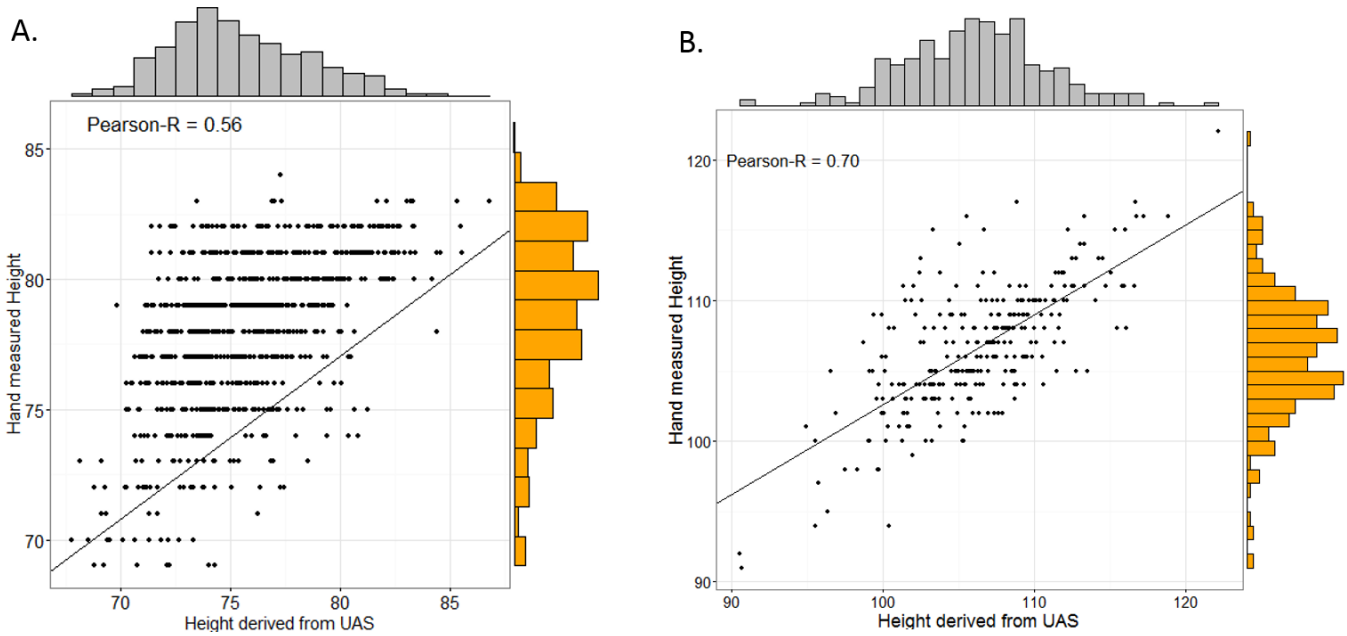

Fig. 2. (A) Correlation between manual height data collected from the drought environment and the height extracted from the unmanned aerial system (UAS, $r = 0.56$). The correlation improves after removing the data points with high SDs (lodged plots) from heights extracted from UAS imagery. (B) Pairwise correlation between manual height data from the first replicate of each trial in irrigated environment and corresponding height extracted from UAS ($r = 0.70$). The correlation improves after removing the data points with high SDs (lodged plots).

as many of the measured VIs exhibited high levels of correlation with the other VIs (Supplemental Tables 2 and 3). Using the plot-level data and a 10-fold cross validation scheme (individual trials as folds), the correlation between the predicted grain yield and observed grain yield was $r = 0.26$ and $r = 0.24$ ($p < 0.001$) for drought and irrigated environments, respectively (Fig. 3), suggesting that PCR could provide some indication of plot yield.

Grain Yield Prediction Using GWR

Because plant breeding trials are inherently spatial in nature, we assessed the use of GWR to predict grain yield. We used a subset of the extracted VIs for variables within the GWR model. The GWR model provides basic variable selection to account for correlated variables that were typical of our VIs. The data were then entered into the GW model using a variable bandwidth setting that minimized the AIC.

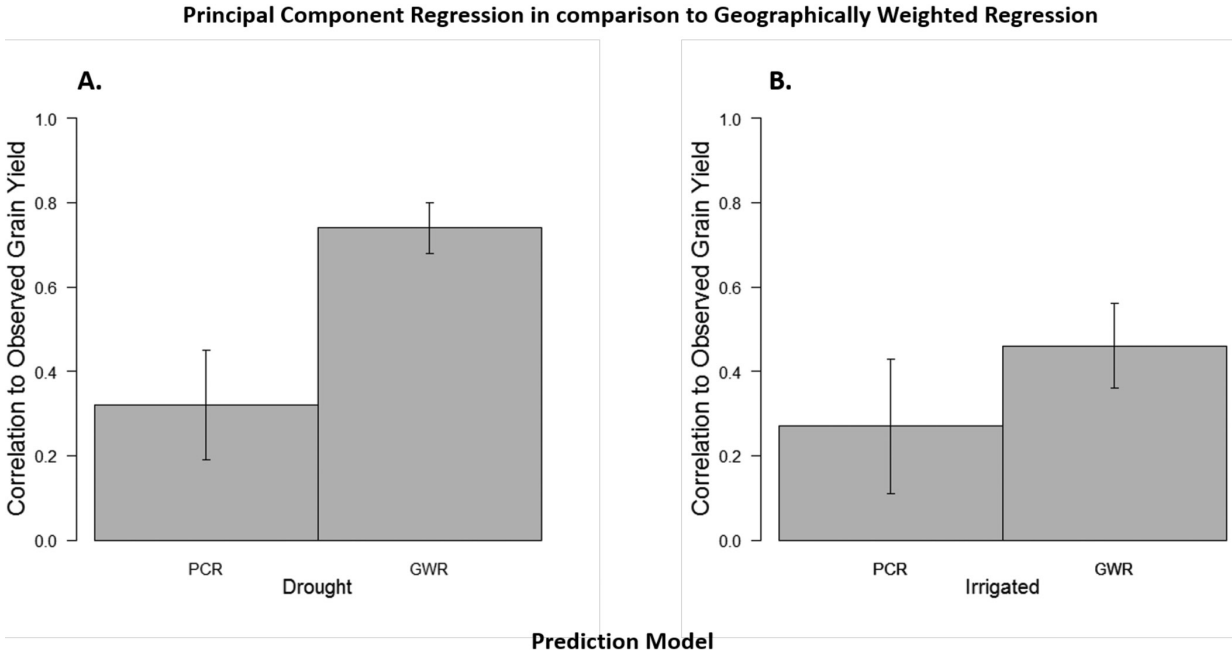

Fig. 3. Prediction accuracy between predicted grain yield and observed grain yield for (A) drought and (B) irrigated environments using principal component regression (PCR) and geographically weighted regression (GWR). (A) For the drought environment, GWR resulted in higher prediction accuracies than PCR ($r = 0.74$ using GWR vs. $r = 0.26$ using PCR). (B) For the irrigated environment, $r = 0.46$ using GWR versus $r = 0.24$ using PCR.

Using cross validation, the average correlations between observed and predicted values were $r = 0.74$ and 0.46 ($p < .001$) for the drought and irrigated environments respectively (Fig. 3). In addition to having higher prediction accuracies than PCR, the RMSE was decreased from 0.45 to 0.14 for the drought environment and 0.45 to 0.2 for the irrigated environment.

In general, GWR resulted in much higher prediction accuracies than PCR. This would be expected, as GWR takes into account the neighborhood (local environment) around the plot, whereas PCR accounts for the entire experiment area with no local flexibility. Higher prediction was observed in both environments for GWR. However, both PCR and GWR followed a similar trend of higher predictive ability in the drought environment with less predictive power in the irrigated environment. We examined the heritability for each observed phenotypic trait (VIs and grain yield) for each of the 10 trials in the study area. In general, heritability was high for all traits (Table 2), suggesting minimal environmental fluctuations. Grain yield had a larger range in heritability between trials in each environment ($H^2 = 0.71–0.96$ for drought grain yield, $H^2 = 0.37–0.87$ for irrigated grain yield) compared with the heritability for the VIs. The lower grain yield heritability would be expected, as grain yield is the result of the entire growing season, whereas daily VIs would represent a single time point of observations. Overall, the irrigated environment had lower heritability for grain yield, which could be contributing to the lower prediction accuracy. The lower predictive ability in the irrigated environment may also be due to the timing of the HTP data collection using UAS within the environments, with sampling dates for the drought environment possibility following more optimal times during the season (Esfandiary et al., 2009). Likewise, the VIs captured by the UAS are likely a better assessment of performance under stress conditions, rather than optimal conditions of the irrigated trials.

CONCLUSION

With the development of new sensors and imaging systems enabling HTP measurements of multiple traits, HTP

Table 2. Broad-sense heritability in 10 trials for vegetation indices (VIs) and grain yield. The VIs† were extracted from Canon S100 at three time points during the growing season for drought and irrigated environments. In the irrigated environment, all the VIs derived from the Canon S100 had higher heritability than the final grain yield.

Broad-sense heritability													
Drought environment													
	2 Mar. 2016				10 Mar. 2015				14 Mar. 2016				
Trial no.	BNDVI	ENDVI	GIPVI	GNDVI	BNDVI	ENDVI	GIPVI	GNDVI	BNDVI	ENDVI	GIPVI	GNDVI	Yield
1	0.94	0.93	0.93	0.93	0.94	0.93	0.89	0.89	0.89	0.85	0.94	0.94	0.88
2	0.91	0.89	0.91	0.91	0.92	0.9	0.88	0.88	0.89	0.85	0.92	0.92	0.71
3	0.93	0.91	0.94	0.94	0.94	0.95	0.88	0.88	0.86	0.82	0.94	0.94	0.85
4	0.92	0.91	0.92	0.92	0.91	0.89	0.93	0.93	0.92	0.87	0.95	0.95	0.92
5	0.89	0.87	0.94	0.94	0.90	0.89	0.91	0.91	0.95	0.93	0.96	0.96	0.96
6	0.88	0.86	0.93	0.93	0.9	0.85	0.91	0.91	0.94	0.88	0.93	0.93	0.78
7	0.96	0.95	0.97	0.97	0.93	0.92	0.88	0.88	0.87	0.82	0.94	0.94	0.91
8	0.95	0.94	0.96	0.96	0.93	0.93	0.90	0.9	0.9	0.88	0.91	0.89	0.89
9	0.90	0.86	0.96	0.96	0.93	0.91	0.94	0.94	0.89	0.85	0.94	0.94	0.9
10	0.91	0.89	0.94	0.94	0.93	0.91	0.93	0.93	0.94	0.88	0.96	0.96	0.92
Mean	0.92	0.90	0.94	0.94	0.92	0.91	0.91	0.91	0.91	0.86	0.94	0.94	0.87
Range	0.88–0.96	0.86–0.95	0.91–0.97	0.91–0.97	0.90–0.94	0.85–0.95	0.88–0.94	0.88–0.94	0.86–0.95	0.82–0.93	0.91–0.96	0.89–0.96	0.71–0.96
Irrigated environment													
	10 Mar. 2016				15 Mar. 2015				8 Apr. 2016				
Trial no.	BNDVI	ENDVI	GIPVI	GNDVI	BNDVI	ENDVI	GIPVI	GNDVI	BNDVI	ENDVI	GIPVI	GNDVI	Yield
1	0.98	0.98	0.94	0.94	0.97	0.96	0.92	0.92	0.88	0.85	0.94	0.94	0.48
2	0.94	0.94	0.91	0.91	0.93	0.93	0.88	0.88	0.93	0.90	0.97	0.97	0.78
3	0.92	0.92	0.90	0.90	0.91	0.91	0.86	0.86	0.92	0.90	0.94	0.94	0.66
4	0.93	0.93	0.90	0.90	0.93	0.94	0.82	0.82	0.94	0.9	0.92	0.92	0.84
5	0.92	0.92	0.87	0.87	0.91	0.91	0.84	0.84	0.9	0.91	0.95	0.95	0.46
6	0.85	0.87	0.80	0.80	0.83	0.85	0.78	0.78	0.96	0.91	0.96	0.96	0.87
7	0.89	0.90	0.75	0.75	0.89	0.92	0.67	0.67	0.96	0.95	0.97	0.97	0.37
8	0.91	0.90	0.89	0.89	0.92	0.93	0.85	0.85	0.85	0.84	0.90	0.90	0.73
9	0.95	0.95	0.94	0.94	0.98	0.98	0.91	0.91	0.92	0.93	0.91	0.91	0.86
10	0.95	0.95	0.91	0.91	0.96	0.96	0.88	0.88	0.86	0.85	0.93	0.93	0.50
Mean	0.92	0.93	0.88	0.88	0.92	0.93	0.84	0.84	0.91	0.89	0.94	0.94	0.66
Range	0.85–0.98	0.87–0.98	0.75–0.94	0.75–0.94	0.83–0.98	0.85–0.98	0.67–0.92	0.67–0.92	0.85–0.96	0.84–0.95	0.90–0.97	0.90–0.97	0.37–0.87

† BNDVI, blue normalized difference VI; ENDVI, enhanced normalized difference VI; GIPVI, green infrared percentage VI; GNDVI, green normalized difference VI.

can advance the scope of scientific studies and expand our understanding of plants. Using a low-cost UAS, we generated spatiotemporal phenotypic data and applied a semiautomated pipeline to extract information from individual wheat plots during the growing season. In this study, we extracted plot-level information on plant height and vegetation indices for wheat breeding lines grown under irrigated and drought conditions and used these measurements to build yield prediction models in the breeding program.

The extracted height from UAS had a high correlation with manual measurements in both environments. Although planting systems (flat vs. bed) and variation in plants' height may have had an effect on estimated readings, our results demonstrate that UAS can be successfully used for measuring plant height in wheat. Following this, we evaluated several prediction models for grain yield using only phenotypic data, with models accounting for spatial variability performing the best. In addition to predicting plant yield, our analysis highlights some of the flexibility in these methods that end users can use by modifying how data can be extracted and classified from the images. For example, dense point cloud classification provides ways to customize the DEM generation step, as the software allows the user to choose the types of objects within the scene to be reconstructed and to indicate the corresponding point class as a source data for DEM generation.

Our study provides strong support of the value of UAS for predicting and evaluating several physiological traits and using this information for overall yield prediction. Application of this technology can enable plant breeders and scientists to enhance their understanding of plants, especially using types of data collected by UAS in genetic studies and genomic prediction models. Through the implementation of in-season yield prediction in early generations of the breeding program, selection decisions could be made before harvest and only selected lines harvested from the field. In addition to using phenotypic data to improve selection decision, this data could also be layered with genomic data, combining the power of both phenotypic and genotypic data, which has been shown to increase prediction accuracy (Rutkoski et al., 2016a). Overall, the rapid measurement of VIs and agronomic traits in-season for large breeding nurseries will provide breeders with additional tools to meet the challenge of increasing genetic gain and deliver superior high-yielding varieties.

Conflict of Interest

The authors declare that there is no conflict of interest.

Supplemental Material Available

Supplemental material for this article is available online.

Acknowledgments

This work was done through the International Maize and Wheat Improvement Center (CIMMYT), Mexico, and was supported by the National Science Foundation under Grant no. IOS-1238187, and through support provided by Feed the Future through the US Agency for International Development, under the terms of Contract no. AID-OAA-A-13-00051. The authors would like to thank three anonymous reviewers for their assistance in improving the manuscript. Any opinions, findings, and conclusions or recommendations expressed in this material are those of the authors and do not necessarily reflect the views of the National Science Foundation or of the US Agency for International Development.

References

Agisoft. 2016. Agisoft PhotoScan user manual: Professional edition, version 1.2. Agisoft, St. Petersburg, Russia. http://www.agisoft.com/pdf/photoscan-pro_1_2_en.pdf (accessed 14 Dec. 2016).

Araya, S., B. Ostendorf, G. Lyle, and M. Lewis. 2013. Crop phenology based on MODIS satellite imagery as an indicator of plant available water content. In: Proceedings of the 20th International Congress on Modelling and Simulation, Adelaide, Australia. 1–6 Dec. 2013. The Modelling and Simulation Society of Australia and New Zealand. p. 1896–1902.

Arnold, J.G., M.A. Weltz, E.E. Alberts, and D.C. Flanagan. 1995. Plant growth component. In: USDA Water Erosion Prediction Project: Tech. Rep. no. 10. USDA, West Lafayette, IN. p. 8.1–8.41.

Babar, M.A., M.P. Reynolds, M. Van Ginkel, A.R. Klatt, W.R. Raun, and M.L. Stone. 2006a. Spectral reflectance indices as a potential indirect selection criteria for wheat yield under irrigation. Crop Sci. 46:578–588. doi:10.2135/cropsci2005.0059

Babar, M.A., M. van Ginkel, R. Klatt, B. Prasad, and M.P. Reynolds. 2006b. The potential of using spectral reflectance indices to estimate yield in wheat grown under reduced irrigation. Euphytica 150:155–172. doi:10.1007/s10681-006-9104-9

Bates, D., M. Maechler, B. Bolker, and S. Walker. 2014. lme4: Linear mixed-effects models using lme4. Cornell Univ. Library, Ithaca, NY.

Bell, M.A., E. Stations, R.A. Fischer, and W. Program. 1994. Guide to plant and crop sampling: Measurements and observations for agronomic and physiological research in small grain cereals. Wheat Spec. Rep. 32. CIMMYT, Mexico, DF.

Braun, H.J., S. Rajaram, and M. Ginkel. 1996. CIMMYT's approach to breeding for wide adaptation. Euphytica 92:175–183. doi:10.1007/BF00022843

Brunsdon, C., A.S. Fotheringham, and M.E. Charlton. 1996. Geographically weighted regression: A method for exploring spatial nonstationary. Geogr. Anal. 28:281–298. doi:10.1111/j.1538-4632.1996.tb00936.x

Cobb, J.N., G. DeClerck, A. Greenberg, R. Clark, and S. McCouch. 2013. Next-generation phenotyping: Requirements and strategies for enhancing our understanding of genotype–phenotype relationships and its relevance to crop improvement. Theor. Appl. Genet. 126:867–887. doi:10.1007/s00122-013-2066-0

Crain, J.L., M.P. Reynolds, and J.A. Poland. 2016. Utilizing high-throughput phenotypic data for improved phenotypic selection of stress adaptive traits in wheat. Crop Sci. 57:648–659. doi:10.2135/cropsci2016.02.0135

Deery, D., J. Jimenez-Berni, H. Jones, X. Sirault, and R. Furbank. 2014. Proximal remote sensing buggies and potential applications for field-based phenotyping. Agronomy 4:349–379. doi:10.3390/agronomy4030349

De La Fuente, G.N., U.K. Frei, and T. Lübberstedt. 2013. Accelerating plant breeding. Trends Plant Sci. 18:667–672. doi:10.1016/j.tplants.2013.09.001

Elshire, R.J., J.C. Glaubitz, Q. Sun, J.A. Poland, K. Kawamoto, E.S. Buckler, and S.E. Mitchell. 2011. A robust, simple genotyping-by-sequencing (gbs) approach for high diversity species. PLoS One 6:e19379. doi:10.1371/journal.pone.0019379

Esfandiary, F., G. Aghaie, and A.D. Mehr. 2009. Wheat yield prediction through agro meteorological indices for ardebil district. Int. J. Biol. Biomol. Agric. Food Biotechnol. Eng. 3:18–21.

Falconer, D.S., and T.F. Mackay. 1996. Introduction to quantitative genetics. 4th ed. Longman, Essex, UK.

Feng, Q., J. Liu, and J. Gong. 2015. Urban flood mapping based on unmanned aerial vehicle remote sensing and random forest classifier: A case of Yuyao, China. Water 7:1437–1455. doi:10.3390/w7041437

Foley, J.A., N. Ramankutty, K.A. Brauman, E.S. Cassidy, J.S. Gerber, M. Johnston et al. 2011. Solutions for a cultivated planet. Nature 478:337–342. doi:10.1038/nature10452

Fotheringham, A.S., C. Brunsdon, and M. Charlton. 2002. Geographically weighted regression: The analysis of spatially varying relationships. Wiley, New York.

Gilmour, A.R., B.R. Cullis, and A.P. Verbyla. 1997. Accounting for natural and extraneous variation in the analysis of field experiments. J. Agric. Biol. Environ. Stat. 2:269–273. doi:10.2307/1400446

Goggin, F.L., A. Lorence, and C.N. Topp. 2015. Applying high-throughput phenotyping to plant–insect interactions: Picturing more resistant crops. Curr. Opin. Insect Sci. 9:69–76. doi:10.1016/j.cois.2015.03.002

Haghighattalab, A. 2014. Orthomosaic generation. Zenodo, Genève, Switzerland. doi:10.5281/zenodo.46734

Haghighattalab, A. 2015. Plot boundary extraction. Zenodo, Genève, Switzerland. doi:10.5281/zenodo.46732

Haghighattalab, A., L. González Pérez, S. Mondal, D. Singh, D. Schinstock, J. Rutkoski et al. 2016. Application of unmanned aerial systems for high throughput phenotyping of large wheat breeding nurseries. Plant Methods 12:35. doi:10.1186/s13007-016-0134-6

Holland, J., W. Nyquist, and C. Cervantes-Martinez. 2003. Estimating and interpreting heritability for plant breeding: An update. Plant Breed. Rev. 22:9–112. doi:10.1002/9780470650202.ch2

Hruska, R., J. Mitchell, M. Anderson, and N.F. Glenn. 2012. Radiometric and geometric analysis of hyperspectral imagery acquired from an unmanned aerial vehicle. Remote Sens. 4:2736–2752. doi:10.3390/rs4092736

Kupfer, J.A., and C.A. Farris. 2007. Incorporating spatial non-stationarity of regression coefficients into predictive vegetation models. Landscape Ecol. 22:837–852. doi:10.1007/s10980-006-9058-2

Liebisch, F., N. Kirchgessner, D. Schneider, A. Walter, and A. Hund. 2015. Remote, aerial phenotyping of maize traits with a mobile multi-sensor approach. Plant Methods 11:9. doi:10.1186/s13007-015-0048-8

Lopes, M.S., and M.P. Reynolds. 2012. Stay-green in spring wheat can be determined by spectral reflectance measurements (normalized difference vegetation index) independently from phenology. J. Exp. Bot. 63:3789–3798. doi:10.1093/jxb/ers071

Lu, B., M. Charlton, P. Harris, and A. Stewart. 2014a. Geographically weighted regression with a non-Euclidean distance metric: A case study using hedonic house price data. Int. J. Geogr. Inf. Sci. 28:660–681. doi:10.1080/13658816.2013.865739

Lu, B., P. Harris, M. Charlton, and C. Brunsdon. 2014b. The GWmodel R package : Further topics for exploring spatial heterogeneity using geographically weighted models. Geospatial Inf. Sci. 17:85–101.

Manjunath, K.R., M.B. Potdar, and N.L. Purohit. 2002. Large area operational wheat yield model development and validation based on spectral and meteorological data. Int. J. Remote Sensing 23:3023–3038. doi:10.1080/01431160110104692

Mennis, J. 2006. Mapping the results of geographically weighted regression. Cartogr. J. 43:171–179. doi:10.1179/000870406X114658

Mevik, B.H., and R. Wehrens. 2007. The pls package: Principal component and partial least squares regression in R. J. Stat. Softw. 18:1–23. doi:10.18637/jss.v018.i02

Mevik, B.H., R. Wehrens, and K.H. Liland. 2013. pls: Partial least squares and principal component regression. R Foundation for Statistical Computing, Vienna, Austria.

Mitchell, A. 2005. The ESRI guide to GIS analysis. Vol. 2: Spatial measurements and statistics. ESRI Press, Redlands, CA.

Mkhabela, M.S., P. Bullock, S. Raj, S. Wang, and Y. Yang. 2011. Crop yield forecasting on the Canadian prairies using MODIS NDVI data. Agric. For. Meteorol. 151:385–393. doi:10.1016/j.agrformet.2010.11.012

Muir, J.F., J. Pretty, S. Robinson, S.M. Thomas, and C. Toulmin. 2010. Food Security : The challenge of feeding 9 billion people. Science 327:812–818. doi:10.1126/science.1185383

Nakaya, T. 2016. Windows application for geographically weighted regression modelling.

Oliver, M.A., and R. Webster. 2015. Geostatistical prediction: Kriging. In: Basic steps in geostatistics: The variogram and kriging. Springer Int. Publ., Wageningen, the Netherlands. p. 43–69.

Piepho, H.-P., and J. Möhring. 2007. Computing heritability and selection response from unbalanced plant breeding trials. Genetics 177:1881–1888. doi:10.1534/genetics.107.074229

Poland, J. 2015. Breeding-assisted genomics. Curr. Opin. Plant Biol. 24:119–124. doi:10.1016/j.pbi.2015.02.009

Prasad, A.K., L. Chai, R.P. Singh, and M. Kafatos. 2006. Crop yield estimation model for Iowa using remote sensing and surface parameters. Int. J. Appl. Earth Obs. Geoinf. 8:26–33. doi:10.1016/j.jag.2005.06.002

QGIS Development Team. 2015. QGIS Geographic Information System. Open Source Geospatial Foundation Project. https://www.qgis.org/ (accessed 14 Dec. 2016).

Raun, W.R., J.B. Solie, G.V. Johnson, M.L. Stone, E.V. Lukina, W.E. Thomason, and J.S. Schepers. 2001. In-season prediction of potential grain yield in winter wheat using canopy reflectance. Agron. J. 93:131–138. doi:10.2134/agronj2001.931131x

Ray, D.K., N.D. Mueller, P.C. West, and J.A. Foley. 2013. Yield trends are insufficient to double global crop production by 2050. PLoS One 8:e66428. doi:10.1371/journal.pone.0066428

Reynolds, M., J. Foulkes, R. Furbank, S. Griffiths, J. King, E. Murchie et al. 2012. Achieving yield gains in wheat. Plant Cell Environ. 35:1799–1823. doi:10.1111/j.1365-3040.2012.02588.x

Reynolds, M., and P. Langridge. 2016. Physiological breeding. Curr. Opin. Plant Biol. 31:162–171. doi:10.1016/j.pbi.2016.04.005

Reynolds, M., Y. Manes, A. Izanloo, and P. Langridge. 2009. Phenotyping approaches for physiological breeding and gene discovery in wheat. Ann. Appl. Biol. 155:309–320. doi:10.1111/j.1744-7348.2009.00351.x

Rischbeck, P., S. Elsayed, B. Mistele, G. Barmeier, and K. Heil. 2016. Data fusion of spectral, thermal and canopy height parameters for improved yield prediction of drought stressed spring barley. Eur. J. Agron. 78:44–59. doi:10.1016/j.eja.2016.04.013

Rosnell, T., and E. Honkavaara. 2012. Point cloud generation from aerial image data acquired by a quadrocopter type micro unmanned aerial vehicle and a digital still camera. Sensors (Basel Switzerland) 12:453–480. doi:10.3390/s120100453

Rutkoski, J., J. Poland, S. Mondal, E. Autrique, L.G. Párez, J. Crossa et al. 2016a. Canopy temperature and vegetation indices from high-throughput phenotyping improve accuracy of pedigree and genomic selection for grain yield in wheat. G3: Genes, Genomes, Genet. 6:2799–2808. doi:10.1534/g3.116.032888

Rutkoski, J., J. Poland, S. Mondal, E. Autrique, L. Gonzalez Perez, J. Crossa et al. 2016b. Predictor traits from high-throughput phenotyping improve accuracy of pedigree and genomic selection for grain yield in wheat. CIMMYT, Mexico, DF.

Salazar, L., F. Kogan, and L. Roytman. 2007. Use of remote sensing data for estimation of winter wheat yield in the United States. Int. J. Remote Sens. 28:3795–3811. doi:10.1080/01431160601050395

Singh, S.P., O.P. Bishnoi, R. Niwas, and M. Singh. 2001. Relationship of wheat grain yield with spectral indices. J. Indian Soc. Remote Sensing 29:93–96. doi:10.1007/BF02989919

Smith, G.M., and E.J. Milton. 1999. The use of the empirical line method to calibrate remotely sensed data to reflectance. Int. J. Remote Sensing 20:2653–2662. doi:10.1080/014311699211994

Sultana, S.R., A. Ali, A. Ahmad, M. Mubeen, S. Ahmad, S. Ercisli, and H.Z.E. Jaafar. 2014. Normalized difference vegetation index as a tool for wheat yield estimation : A case study from Faisalabad, Pakistan. Sci. World J. 2014:725326. doi:10.1155/2014/725326

Teal, R.K., B. Tubana, K. Girma, K.W. Freeman, D.B. Arnall, O. Walsh, and W.R. Raun. 2006. In-season prediction of corn grain yield potential using normalized difference vegetation index. Agron. J. 98:1488–1494. doi:10.2134/agronj2006.0103

Tester, M., and P. Langridge. 2010. Breeding technologies to increase crop production in a changing world. Science 327:818–822. doi:10.1126/science.1183700

Tobler, A.W.R. 1970. A computer movie simulating urban growth in the Detroit region. Econ. Geogr. 46:234–240. doi:10.2307/143141

USDA. 2016. World agricultural supply and demand estimates. Off. Chief Econ., USDA. http://www.usda.gov/oce/commodity/wasde/latest.pdf (accessed 14 Dec. 2016).

Wang, K., C. Zhang, and W. Li. 2012. Comparison of geographically weighted regression and regression kriging for estimating the spatial distribution of soil organic matter. GIsci. Remote Sens. 49:915–932. doi:10.2747/1548-1603.49.6.915

Wang, L., Y. Tian, X. Yao, Y. Zhu, and W. Cao. 2014. Predicting grain yield and protein content in wheat by fusing multi- sensor and multi-temporal remote-sensing images. Fields Crops Res. 164:178–188. doi:10.1016/j.fcr.2014.05.001

White, J., P. Andrade-Sanchez, M.A. Gore, K.F. Bronson, T.A. Coffelt, M.M. Conley et al. 2012. Field-based phenomics for plant genetics research. Field Crops Res. 133:101–112. doi:10.1016/j.fcr.2012.04.003

You, X., J. Meng, M. Zhang, and T. Dong. 2013. Remote sensing based detection of crop phenology for agricultural zones in china using a new threshold method. Remote Sens. 5:3190–3211. doi:10.3390/rs5073190

Zadoks, J.C., T.T. Chang, and C.F. Konzak. 1974. A decimal code for the growth stages of cereals. Weed Res. 14:415–421. doi:10.1111/j.1365-3180.1974.tb01084.x